JOURNAL OF CHEMICAL & ENGINEERING DATA

ARTICLE

pubs.acs.org/jced

Adsorption of Methyl Orange from Aqueous Solution on Hydrothermal Synthesized Mg−Al Layered Double Hydroxide

Lunhong Ai,* Chunying Zhang, and Lanying Meng

Chemical Synthesis and Pollution Control Key Laboratory of Sichuan Province, College of Chemistry and Chemical Engineering, China West Normal University, Nanchong 637002, People's Republic of China

ABSTRACT: In this study, we presented the efficiently adsorptive removal of organic dye, methyl orange (MO), from aqueous solution with the hydrothermal synthesized Mg−Al layered double hydroxide (LDH). The as-obtained product was characterized by X-ray diffraction (XRD), Fourier transformation infrared spectroscopy (FTIR), and scanning electron microscopy (SEM). The adsorption characteristics of MO onto the Mg−Al LDH were evaluated in a batch adsorption process and systematically investigated by different experimental parameters, such as initial dye concentration, contact time, and solution pH. The adsorption kinetics were analyzed by pseudofirst-order, pseudosecond-order, Elovich, intraparticle diffusion, and Boyd models, which were well-described by the pseudosecond-order model. The equilibrium adsorption data were interpreted using the Langmuir, Freundlich, and Temkin isotherm models, which fitted well to both the Langmuir and Freundlich models. The monolayer adsorption capacity of the Mg−Al LDH toward MO was found to be 0.453 mol·kg^{-1}. These findings suggested that the LDH could be regarded as a promising adsorbent for the removal of anionic dye in wastewaters.

1. INTRODUCTION

Nowadays, organic contaminations from a variety of sources have become a global concern because of their impact on public health. In particular, organic dye pollutants by various chemical and textile industries have received great attention due to increasing the environmental risk when they are discarded into water, which can not only cause aesthetic problems, but also exhibit high biotoxicity and potential mutagenic and carcinogenic effects.[1,2] Thus, the efficient removal of such kinds of pollutants before discharging to the receiving water bodies is becoming a crucial issue. However, the nondegradable nature and stability toward light and/or oxidizing agents of dyes complicates the selection of a suitable method for removal. Several methods have been developed to treat the dye-containing effluents, including biological treatment,[3] coagulation/flocculation,[4] ozone treatment,[5] chemical oxidation,[6] membrane filtration,[7] ion exchange,[8] photocatalysis,[9] and adsorption.[10] Among these methods, adsorption is a reliable alternative due to its simplicity, high efficiency, and ease of operation as well as the availability of a wide range of adsorbents. Various kinds of materials including activated carbon,[11] zeolite,[12] fly ash,[13] clay,[14] polymer,[15] and byproduct[16] have been found to be capable of removing dyestuffs from wastewater. In view of pollutant control at present, it is still indispensible to exploit the new adsorbent materials with high adsorption capacities and removal efficiencies.

Layered double hydroxides (LDHs), well-known as anionic clays or hydrotalcite-like compounds, are a large class of natural and synthetic materials, which have received considerable attention in recent years due to their promising applications in many fields, such as in catalysts and catalyst supports, adsorbents, separation materials, additives in plastics, and biological and pharmaceutical materials.[17−20] LDHs are represented by the general formula $[M^{2+}_{1-x}M^{3+}_{x}(OH)_2](A_{x/n}{}^{n-})\cdot mH_2O$, where M^{2+} is a divalent cation (Mg^{2+}, Zn^{2+}, Cu^{2+}, Ni^{2+}, Co^{2+}, etc.), M^{3+} is a trivalent cation (Al^{3+}, Fe^{3+}, Cr^{3+}, etc.), and A^{n-} is an interlayer anion ($CO_3{}^{2-}$, $SO_4{}^{2-}$, $NO_3{}^{-}$, Cl^{-}, OH^{-}, etc.); x is a ratio between di- and trivalent cations with various values between 0.2 and 0.33.[21,22] The structure consists of brucite-like layers built up from edge-sharing $M(OH)_6$ octahedra. Interestingly, a partial and isostructural M^{2+} to M^{3+} substitution would induce a positive charge for these layers, balanced with the negatively charged interlayer region containing anions and water molecules.[21] This remarkable structure feature allows LDHs to have a powerful ability to capture organic and/or inorganic anions in aqueous solutions. In this regard, the LDHs were thereby spread to the field of water treatment. To date, the adsorptive removal of various pollutants in water on this kind of materials has been demonstrated.[23−27]

To our knowledge, there is little report regarding the removal of methyl orange (MO) over the hydrothermal synthesized Mg−Al LDH until now. The objectives of this study were to (i) hydrothermally synthesize and characterize the Mg−Al LDH; (ii) investigate the adsorption behavior of MO onto the Mg−Al LDH; and (iii) analyze the adsorption kinetics and isotherms of adsorption of MO onto the Mg−Al LDH using the theoretical models.

2. EXPERIMENTAL SECTION

2.1. Chemicals. All of the reagents were of analytical grade with the mass fraction purity of 0.99 and used as received without further purification. $Al(NO_3)_3\cdot 9H_2O$, $Mg(NO_3)_2\cdot 6H_2O$, and MO were purchased from Sinopharm Chemical Reagent Co., Ltd. (Shanghai, China).

2.2. Preparation of the Mg−Al LDH Adsorbent. The Mg−Al LDH was synthesized by a hydrothermal route according

Received: July 18, 2011
Accepted: October 11, 2011
Published: October 26, 2011

dx.doi.org/10.1021/je200743u | J. Chem. Eng. Data 2011, 56, 4217–4225

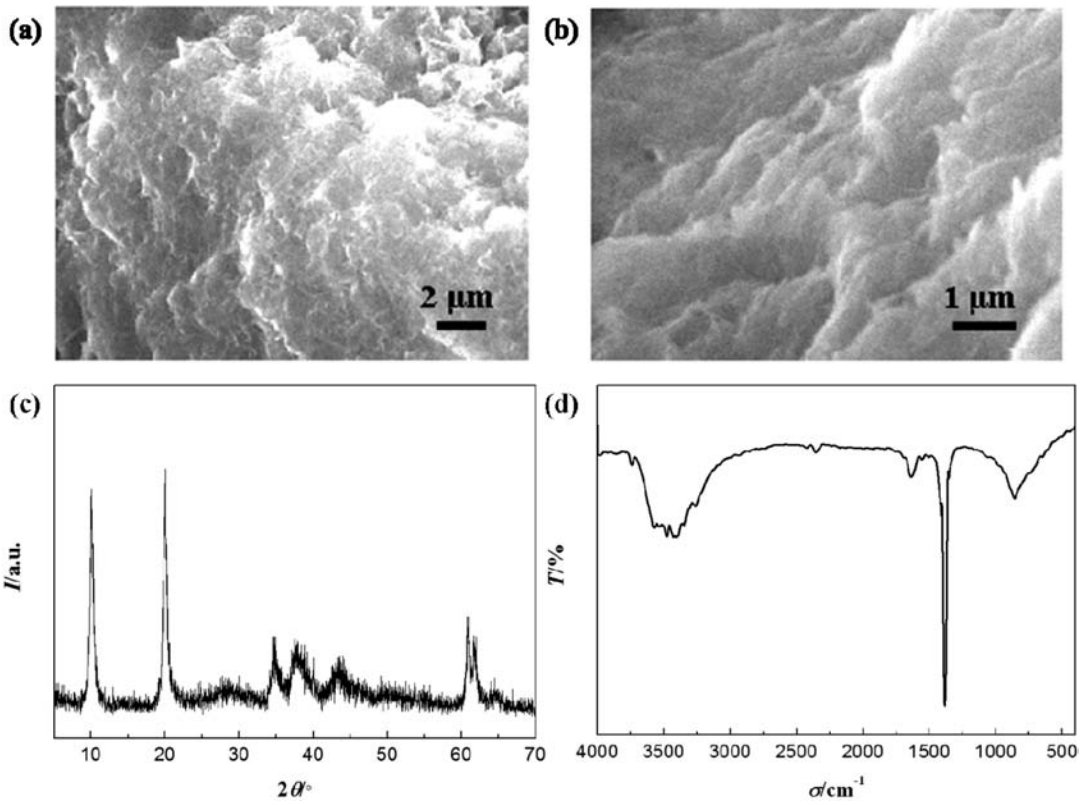

Figure 1. (a,b) SEM images, (c) XRD pattern (diffraction peak intensity I versus diffraction angle 2θ), and (d) FTIR spectrum (wavenumber σ versus transmittance T) of the as-prepared Mg−Al LDH.

to Hu's report with tiny modifications.[28] Typically, 1 mmol of $Al(NO_3)_3 \cdot 9H_2O$ and 2 mmol of $Mg(NO_3)_2 \cdot 6H_2O$ were dissolved in 50 cm^3 of deionized water to obtain a clear solution under magnetic stirring. A desired amount of aqueous ammonia was added to above mixture solution to adjust the pH value to about 11.0. The resulting mixture was stirred for another 1800 s and then transferred into a 100 cm^3 Teflon-lined stainless steel autoclave and kept at 473 K for $7.2 \cdot 10^4$ s followed by cooling to ambient temperature naturally. The white precipitate was centrifuged, washed with ethanol and distilled water several times, and finally dried at 333 K in a vacuum oven. The Mg^{2+} and Al^{3+} contents of the adsorbent were analyzed using an IRIS Intrepid II XDL inductively coupled plasma atomic emission spectrometer (ICP-AES) after dissolving the sample in nitric acid. The carbon and nitrogen contents were measured in a Heraeus Vario EL-III elemental analyzer. The chemical formula of the adsorbent were determined to be $Mg_{0.67}Al_{0.33}(OH)_2(NO_3)_{0.25}(CO_3)_{0.04}$.

2.3. Adsorption Experiments. Batch adsorption experiments were carried out in a thermostatted shaker with a shaking speed of 15.7 $rad \cdot s^{-1}$ using 100 cm^3 Erlenmeyer flasks and conducted in duplicate. In general, 0.02 ± 0.0001 g of the Mg−Al LDH were added into 50 ± 0.1 cm^3 of MO solutions of desired initial concentrations at natural pH of 6.5 ± 0.1 in flask and agitated in a temperature-controlled shaker at 298 ± 1 K. At predetermined time intervals, the samples were removed from the solution by centrifugation. The effect of pH on the adsorption of MO onto the Mg−Al LDH was studied over a pH range of (2.0 ± 0.1 to 10.0 ± 0.1) with a contact time of $7.2 \cdot 10^3$ s. The pH was adjusted by adding aqueous solutions of 0.1 $mol \cdot kg^{-1}$ HCl or 0.1 $mol \cdot kg^{-1}$ NaOH. The adsorption kinetics was determined by the analysis of the adsorption capacity from the aqueous solution at different time intervals. For adsorption isotherms, MO solution of different concentrations was incubated with the adsorbent under agitation until the equilibrium was achieved. The concentration of dye was determined at 460 nm for MO using a UV−vis spectrophotometer (Shimadzu, UV-2550). The equilibrium adsorption capacity of MO onto the Mg−Al LDH was evaluated by using the mass balance equation:

$$q = \frac{(C_0 - C_e)V}{m} \quad (1)$$

where C_0 and C_e are the initial and equilibrium concentrations of dye, m is the mass of the Mg−Al LDH, and V is the volume of solution.

2.4. Characterization. The powder X-ray diffraction (XRD) measurements were recorded on a Rigaku Dmax/Ultima IV diffractometer with monochromatized Cu Kα radiation (λ = 0.15418 nm). The morphology was observed with a JSM-6510 scanning electron microscope (SEM). The Fourier transform infrared (FTIR) spectroscopy was measured on Nicolet 6700 FTIR spectrometric analyzer using KBr pellets. A pHS-3C digital pH meter (Rex Instruments Factory, Shanghai, China) was employed for the pH measurements. The point of zero charge (pH_{PZC}) of the Mg−Al LDH was determined by the solid addition method. To a series of 100 cm^3 conical flasks, 45 cm^3 of 0.1 $mol \cdot kg^{-1}$ NaCl solution was transferred. The initial pH values (pH_i) of the solution were adjusted from (1.0 to 11.0) by adding either 0.1 $mol \cdot kg^{-1}$ HCl or 0.1 $mol \cdot kg^{-1}$ NaOH. The total volume of the solution in each flask was made exactly to 50 cm^3 by adding the NaCl solution. Then, 0.1 g of the Mg−Al LDH was added to each flask, and the mixtures were agitated at

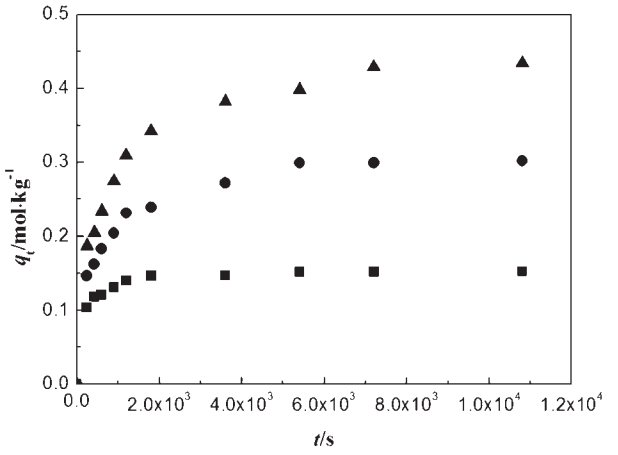

Figure 2. Adsorption capacity q_t versus time t for the adsorption of MO onto the Mg−Al LDH at different initial MO concentrations (square: $6.11 \cdot 10^{-5}$ mol·kg^{-1}, circle: $1.22 \cdot 10^{-4}$ mol·kg^{-1}, triangle: $1.83 \cdot 10^{-4}$ mol·kg^{-1}).

15.7 rad·s^{-1}. After $1.73 \cdot 10^5$ s, the final pH values (pH_f) of the solutions were measured. The difference between the initial and final pH values ($\Delta pH = pH_i - pH_f$) was plotted against the pH_i. The point of intersection of the resulting curve with abscissa, at which $\Delta pH = 0$, gave the pH_{PZC}.

3. RESULTS AND DISCUSSION

3.1. Characterization of the As-Prepared Adsorbent. The morphology of the as-prepared adsorbent was observed by scanning electron microscopy (SEM). Figure 1a,b shows the typical SEM images of the Mg−Al LDH, which consisted of the aggregation of small platelets with a smooth surface. The crystalline structure of the as-prepared adsorbent was also determined by XRD. Figure 1c shows the XRD pattern of the Mg−Al LDH. It exhibited the characteristic diffractions of well-crystallized hydrotalcite-like LDHs. A series of (00l) peaks indexed as (003), (006), and (009) appearing as symmetric lines at low 2θ angle correspond to the basal spacing, indicating the presence of an ordered stacking sequence. The structure of the as-prepared adsorbent was further determined by the FTIR spectroscopy. Figure 1d shows the FTIR spectrum of the Mg−Al LDH. The characteristic peaks are located at 3440 cm^{-1} (the stretching vibration of O−H), 1620 cm^{-1} (the bending vibration of O−H), and 1377 cm^{-1} (the bending vibration of N−O). In addition, the peaks in the range of (400 to 900) cm^{-1} are assigned to the lattice vibration modes of M−O and M−OH.[28]

3.2. Effect of Contact Time and Initial MO Concentration. MO was chosen as a model dye to assess the adsorption capacity of the as-prepared Mg−Al LDH. A series of systematic experiments have been performed to examine the MO adsorption with the Mg−Al LDH in aqueous solution. Figure 2 shows the effect of contact time on the adsorption capacity of MO onto the Mg−Al LDH at different initial concentrations. It can be seen that the adsorption rates of MO onto the Mg−Al LDH were considerably rapid within the first $1.8 \cdot 10^3$ s for all of the concentrations. Thereafter, the adsorption proceeded slowly with contact time before reaching a plateau value after $7.2 \cdot 10^3$ s. The high adsorption rate within the initial $1.8 \cdot 10^3$ s was attributed to the adequate free adsorptive sites and a high dye concentration gradient. The removal efficiencies were found to be 99.9 %, 98.9 %, and 95.5 % at the initial concentrations of ($6.11 \cdot 10^{-5}$, $1.22 \cdot 10^{-4}$, and $1.83 \cdot 10^{-4}$) mol·kg^{-1}, respectively, demonstrating the high efficiency of the Mg−Al LDH for the MO adsorption in aqueous solutions. On the other hand, the adsorption process was also found to be closely dependent on the initial concentrations. The amount of MO adsorbed increased evidently with the increase in initial concentration. This could be a result of an increase in the driving force of concentration gradient to overcome the mass transfer resistance of the dye between the aqueous phases and the solid phases with the increase in the initial concentration.[29−31]

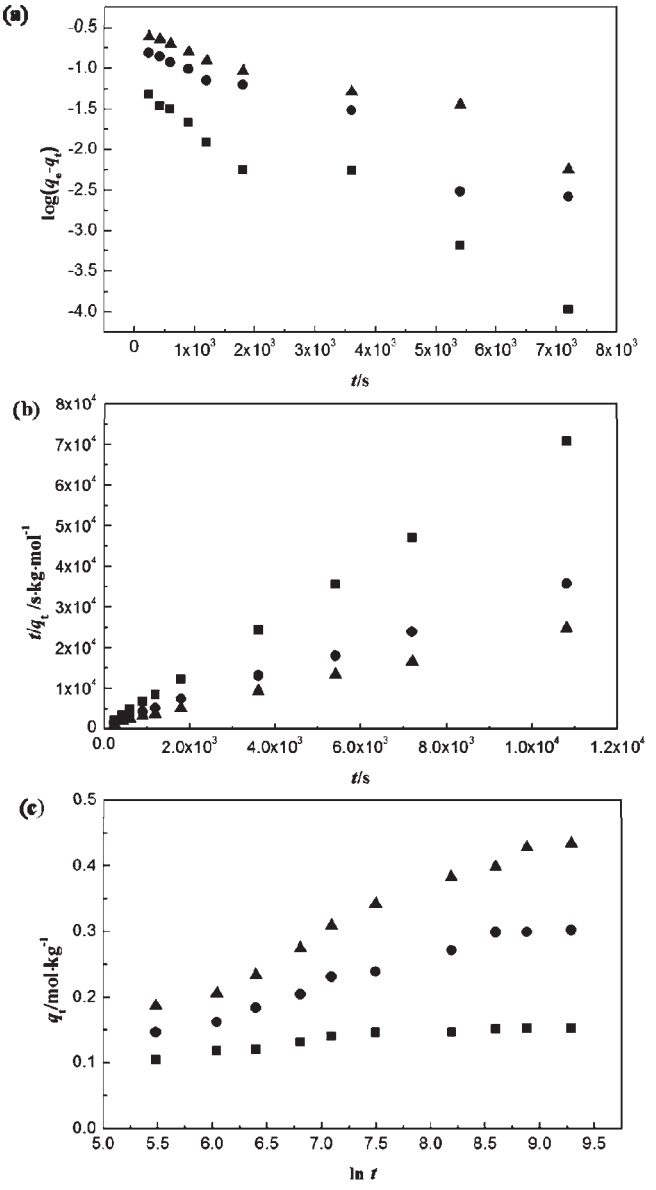

Figure 3. (a) Pseudofirst-order, (b) pseudosecond-order, and (c) Elovich kinetics for the adsorption of MO onto the Mg−Al LDH (square: $6.11 \cdot 10^{-5}$ mol·kg^{-1}, circle: $1.22 \cdot 10^{-4}$ mol·kg^{-1}, triangle: $1.83 \cdot 10^{-4}$ mol·kg^{-1}). q_e: adsorption capacity of MO onto the adsorbent at equilibrium, q_t: adsorption capacity of MO onto the adsorbent at time t.

3.3. Adsorption Kinetics. To understand the detailed characteristics of the adsorption process, the various kinetic models, namely, pseudofirst-order, pseudosecond-order, Elovich, Weber's

dx.doi.org/10.1021/je200743u |J. Chem. Eng. Data 2011, 56, 4217–4225

Table 1. Kinetic Parameters of the Adsorption of MO onto the Mg−Al LDH

		pseudofirst-order			pseudosecond-order			Elovich		
C_0	$q_{e,exp}$[a]	k_1	$q_{e,cal}$		k_2	$q_{e,cal}$		α	β	
mol·kg^{-1}	mol·kg^{-1}	s^{-1}	mol·kg^{-1}	R^2	kg· mol^{-1}·s^{-1}	mol·kg	R^2	mol·kg^{-1}·s^{-1}	kg·mol^{-1}	R^2
$6.11\cdot10^{-5}$	0.152 ± 0.019	$8.03\cdot10^{-4}$	0.046	0.9550	0.048	0.155	0.9999	$36.7\cdot10^{-3}$	78.99	0.8729
$1.22\cdot10^{-4}$	0.300 ± 0.033	$6.23\cdot10^{-4}$	0.177	0.9527	0.007	0.315	0.9991	$4.80\cdot10^{-3}$	22.18	0.9754
$1.83\cdot10^{-4}$	0.429 ± 0.015	$4.73\cdot10^{-4}$	0.261	0.9429	0.004	0.454	0.9988	$3.85\cdot10^{-3}$	14.11	0.9798

[a] The expanded uncertainty was calculated using a coverage factor of 2, which gives a level of confidence of approximately 95 %.

intraparticle diffusion, and Boyd's kinetic models, were applied to identify the dynamics of the adsorption process.

The pseudofirst-order kinetic model assumes that the rate of change of solute uptake with time is directly proportional to difference in saturation concentration and the amount of solid uptake with time, which is generally applicable over the initial stage of an adsorption process. A linear form of the Lagergren's pseudofirst-order equation can be expressed as:[32]

$$\log(q_e - q_t) = \log q_e - \frac{k_1 t}{2.303} \quad (2)$$

where k_1 is the pseudofirst-order rate constant and q_e and q_t are the adsorption capacity of MO onto the adsorbent at equilibrium and at time t, respectively. The parameters k_1 and q_e were determined from the plots of log $(q_e - q_t)$ versus t (Figure 3a) and are summarized in Table 1. The values of the correlation coefficients (R^2) for the pseudofirst-order model obtained are not high at the whole concentration range. Moreover, large differences between experimental ($q_{e,exp}$) and calculated ($q_{e,cal}$) values of the equilibrium adsorption capacity were also observed, which indicates that the adsorption of MO onto the Mg−Al LDH did not obey the pseudofirst-order model.

The pseudosecond-order kinetic model is based on the assumption that the rate-limiting step is chemical sorption or chemisorption and predicts the behavior over the whole range of adsorption. The linear form of pseudosecond-order kinetic model is expressed as:[33]

$$\frac{t}{q_t} = \frac{1}{k_2 q_e^2} + \frac{t}{q_e} \quad (3)$$

where k_2 is the pseudosecond-order adsorption rate constant. The values of k_2 and q_e can be calculated from the slope and intercept of plots of t/q_t versus t (Figure 3b) and are given in Table 1. At all of the studied initial concentrations, the pseudo-second-order model showed a good fit with experimental data ($R^2 > 0.99$). The values of $q_{e,cal}$ also appeared to be very close to the experimentally observed values of $q_{e,exp}$. This finding suggests that the adsorption kinetics followed the pseudosecond-order model. Similar kinetics was observed in the adsorption of dye onto other LDH-based adsorbents.[34] The equilibrium adsorption capacity ($q_{e,cal}$) increased with increasing the initial concentration, attributed to the relatively strong driving force of the concentration gradient at high initial concentrations. Additionally, the pseudosecond-order rate constants (k_2) values decreased from (0.048 to 0.004) kg·mol^{-1}·s^{-1}, which can be ascribed to the lower competition for the adsorption surface sites at lower concentration.[35]

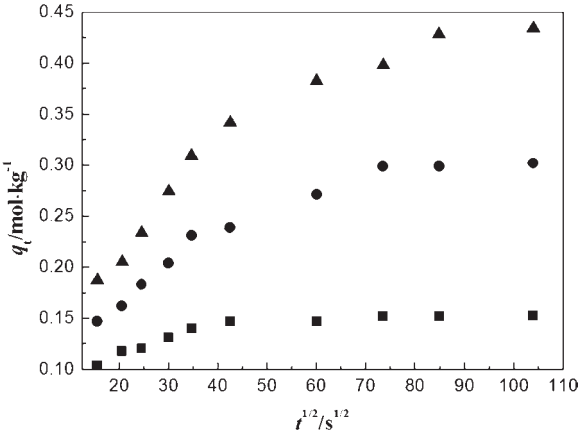

Figure 4. Intraparticle diffusion plots of adsorption capacity q_t versus the square root of time $t^{1/2}$ for the adsorption of MO onto the Mg−Al LDH (square: $6.11\cdot10^{-5}$ mol·kg^{-1}, circle: $1.22\cdot10^{-4}$ mol·kg^{-1}, triangle: $1.83\cdot10^{-4}$ mol·kg^{-1}).

The Elovich kinetic model is often used to interpret the kinetics of adsorption and successfully describe second-order kinetics assuming that the actual solid surfaces are energetically heterogeneous, which is given in the following equation:[36]

$$q_t = \frac{1}{\beta}\ln(\alpha\beta) + \frac{1}{\beta}\ln t \quad (4)$$

where α is the initial adsorption rate and β is the desorption constant. The experimental data were analyzed by the Elovich equation, as shown in Figure 3c. By plotting ln t versus q_t, the constants can be obtained from the slope and intercept of the plot. The correlation coefficients (R^2) were obtained in the range of (0.8729 to 0.9798) for all of the concentrations, which were lower than those of the pseudosecond-order model shown in Table 1.

Considering that the pseudofirst-order, pseudosecond-order, and Elovich kinetic models could not identify the diffusion mechanism, the kinetic data were further analyzed by Weber's intraparticle diffusion model, which can be described as:[37]

$$q_t = k_i t^{1/2} + C_i \quad (5)$$

where k_i is the intraparticle diffusion rate constant and C_i is the intercept. The value of C relates to the thickness of the boundary layer. The larger C implies the greater effect of the boundary

Table 2. Intraparticle Diffusion Model Parameters of the Adsorption of MO onto the Mg−Al LDH

intraparticle diffusion model								
C_0	$k_{i,1}$	C_1		$k_{i,2}$	C_2		Boyd model	
mol·kg^{-1}	mol·kg^{-1}·s$^{-1/2}$	mol·kg^{-1}	R^2	mol·kg^{-1}·s$^{-1/2}$	mol·kg^{-1}	R^2	linear equation	R^2
$6.11\cdot10^{-5}$	$1.81\cdot10^{-3}$	0.078	0.9719	$1.06\cdot10^{-4}$	0.142	0.7004	$B_t = 0.70871t + 8.02903\cdot10^{-4}$	0.9550
$1.22\cdot10^{-4}$	$4.40\cdot10^{-3}$	0.076	0.9874	$1.04\cdot10^{-3}$	0.206	0.7383	$B_t = 0.03916t + 6.23142\cdot10^{-4}$	0.9527
$1.83\cdot10^{-4}$	$6.55\cdot10^{-3}$	0.078	0.9800	$1.55\cdot10^{-3}$	0.284	0.9098	$B_t = 0.01231t + 4.74465\cdot10^{-4}$	0.9428

layer. According to this model, the plots of q_t versus $t^{1/2}$ should be linear if intraparticle diffusion is involved in the adsorption process, and if these lines pass through the origin then intraparticle diffusion is the rate-controlling step.[38] However, if the data exhibit multilinear plots, then two or more steps simultaneously operate the adsorption process. Figure 4 shows the q_t versus $t^{1/2}$ plot at different initial concentrations. For all of the concentrations, two linear regions were observed, indicating that more than one process affected the adsorption process of MO onto the Mg−Al LDH.[39] The first linear section was a diffusion adsorption stage correlated to the diffusion of dye through the solution to the external surface of adsorbent (film diffusion). The second linear portion was a gradual adsorption stage corresponding to intraparticle diffusion of dye molecules through the pores of adsorbent (intraparticle diffusion). In addition, none of the lines passing through the origin reveal that the intraparticle diffusion was not the only rate-controlling step for the whole adsorption process. Additionally, the values of intraparticle rate constant $k_{i,1}$ and $k_{i,2}$ at different initial concentrations are also listed in Table 2. It is clear that both $k_{i,1}$ and $k_{i,2}$ values increased with increasing initial dye concentration. It can be explained by the growing effect of driving force that led to reducing the diffusion of dye molecules in the boundary layer and enhancing the diffusion in the solid. The $k_{i,1}$ values greater than $k_{i,2}$ values suggested that the film diffusion step was an important step for the adsorption of MO onto the Mg−Al LDH. During the adsorption process, MO molecules were initially adsorbed by the exterior surface of the adsorbent. When the adsorption at the exterior surface reached the saturation, MO molecules further entered the pores within the particles and were subsequently adsorbed by the interior surfaces. It is reasonably expected that the diffusion resistance was considerably increased in the interior adsorption process, thus resulting in a decrease in diffusion rate.

To establish the actual rate-controlling step involved in the overall adsorption process, the adsorption kinetic data were further analyzed by the Boyd kinetic model, which is expressed as:[40]

$$F = 1 - \frac{6}{\pi^2}\exp(-B_t) \tag{6}$$

where F is the fraction of solute adsorbed at different time t and B_t is a mathematical function of F and is given by

$$F = \frac{q_t}{q_e} \tag{7}$$

Substituting eq 7 in eq 6, the kinetic expression can be represented as

$$B_t = -0.4977 - \ln(1 - F) \tag{8}$$

According to this model, if the plot of B_t versus t is a straight line passing through the origin, then the rate-limiting step in the adsorption process is the intraparticle diffusion and vice versa. As shown in Figure 5, the plots of the relationship between B_t and t were linear for the adsorption of MO onto the Mg−Al LDH ($R^2 > 0.94$) but did not pass through the origin for different initial dye concentrations (Table 2), reflecting that film diffusion was the rate-controlling step in the adsorption process.

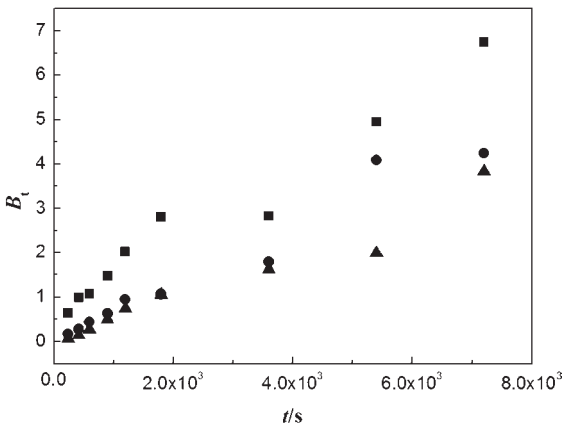

Figure 5. Plots of Boyd parameter B_t versus time t for the adsorption of MO onto the Mg−Al LDH (square: $6.11\cdot10^{-5}$ mol·kg^{-1}, circle: $1.22\cdot10^{-4}$ mol·kg^{-1}, triangle: $1.83\cdot10^{-4}$ mol·kg^{-1}).

3.4. Adsorption Isotherms. Adsorption isotherms provide qualitative information on the capacity of the adsorbent as well as the nature of the solute−surface interaction. Figure 6 shows the adsorption isotherms of MO onto the Mg−Al LDH. The adsorption capacities of MO increased with increasing the dye concentration. Also, the shape of the isotherm revealed L-behavior according to the Giles classification,[41] confirming a high affinity between Mg−Al LDH and the dye molecule.

In our present study, Langmuir,[42] Freundlich,[43] and Temkin[44] isotherms were used to describe the experimental data. The Langmuir isotherm theory assumes monolayer coverage of adsorbate over a homogeneous adsorbent surface. A basic assumption is that adsorption takes place at specific homogeneous sites within the adsorbent. Once a dye molecule occupies a site, no further adsorption can take place at that site. The Langmuir isotherm is expressed as

$$\frac{C_e}{q_e} = \frac{1}{bq_m} + \frac{C_e}{q_m} \tag{9}$$

where b is Langmuir constant and q_m is the Langmuir monolayer adsorption capacity. The parameters q_m and b were calculated from the slope and intercept of the linear plot of C_e/q_e versus C_e (Figure 7a) and are shown in Table 3. The correlation coefficient of the isotherm is relative high (R^2 = 0.9937), which indicates

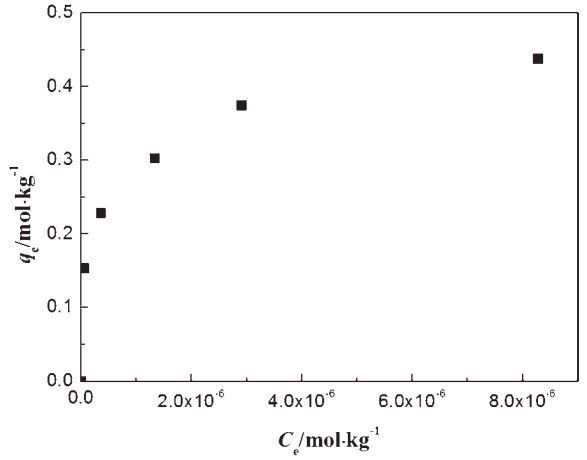

Figure 6. Equilibrium adsorption capacity q_e versus equilibrium concentrations C_e for the adsorption of MO onto the Mg−Al LDH.

that the Langmuir model is suitable for describing the adsorption equilibrium of MO onto the Mg−Al LDH. The monolayer adsorption capacity determined from the Langmuir isotherm is 0.453 mol·kg^{-1}. In comparison with the adsorption capacities of other adsorbents (Table 4), the adsorption capacity of Mg−Al LDH was found to be better than the most other adsorbents reported in the literature.[15,45−49]

The essential characteristics of the Langmuir isotherm can be expressed in terms of a dimensionless constant separation factor R_L that is given by:[50]

$$R_L = \frac{1}{1 + bC_0} \tag{10}$$

The value of R_L indicates the shape of the isotherm to be either unfavorable ($R_L > 1$), linear ($R_L = 1$), favorable ($0 < R_L < 1$), or irreversible ($R_L = 0$).[51] The calculated R_L values at different initial concentration of MO are in the range of (0.0022 to 0.0066), which lie between 0 and 1, thereby confirming that the adsorption is a favorable process. In addition, the low R_L values implied that the interaction of dye molecules with Mg−Al LDH might be relatively strong.[52,53]

The Freundlich isotherm is an empirical equation assuming that the adsorption process takes place on heterogeneous surfaces, and adsorption capacity is related to the concentration of dye at equilibrium. The Freundlich isotherm is described as:

$$\log q_e = \log K_f + \frac{1}{n}\log C_e \tag{11}$$

where K_f is roughly an indicator of the adsorption capacity and $1/n$ is the adsorption intensity. Freundlich constants K_f and n can be obtained from the intercept and the slope of the linear plot of log q_e versus log C_e (Figure 7b). As shown in Table 3, the correlation coefficient (R^2 = 0.9952) reflects that the experimental data agree with the Freundlich model. The Freundlich constant n gives an idea for the favorability of the adsorption process. The value of n should be less than 10 and higher than unity for favorable adsorption conditions. It was found that the value of n for Freundlich model in this case was greater than 1, indicating that the adsorption of MO onto the Mg−Al LDH was a favorable.

The Temkin isotherm assumes that the heat of adsorption of all of the molecules in the layer decreases linearly with the

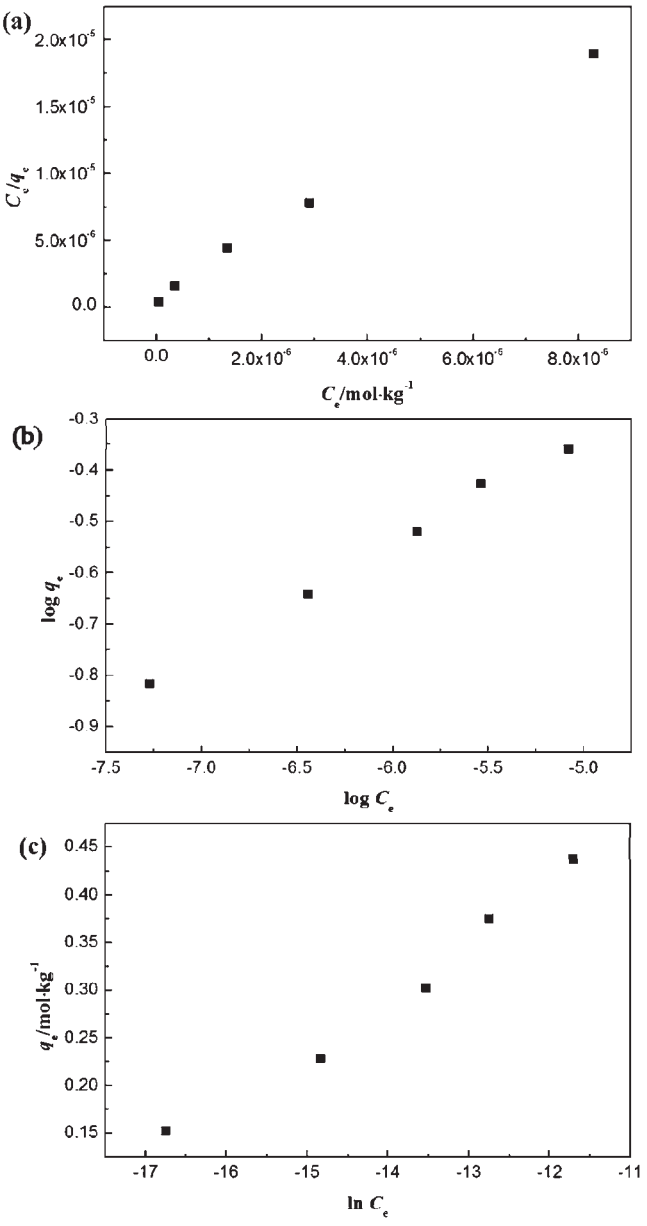

Figure 7. Adsorption isotherm of the adsorption of MO onto the Mg−Al LDH: (a) Langmuir model, (b) Freundlich model, and (c) Temkin model. q_e: equilibrium adsorption capacity, C_e: equilibrium concentrations.

coverage of molecules due to the adsorbate−adsorbate repulsions and the adsorption of adsorbate is uniformly distributed[54] and that the fall in the heat of adsorption is linear rather than logarithmic. The Temkin equation is given by:

$$q_e = B_T \ln A_T + B_T \ln C_e \tag{12}$$

where $B_T = (RT)/b_T$, T is the absolute temperature, and R is the universal gas constant (8.3145 J·mol^{-1}·K^{-1}). The constant b_T is related to the heat of adsorption, and A_T is the equilibrium binding constant corresponding to the maximum binding energy. The slope and the intercept from a plot of q_e versus ln C_e determined the isotherm constants A_T and B_T (Figure 7c). The correlation coefficient (R^2 = 0.9703) of the Temkin isotherm was lower than that obtained for the Langmuir and Freundlich

Table 3. Isotherm Parameters for the Adsorption of MO onto the Mg−Al LDH

Langmuir			Freundlich			Temkin		
b	q_m					b_T	A_T	
kg·mol^{-1}	mol·kg^{-1}	R^2	K_f	n	R^2	J·mol	kg·mol^{-1}	R^2
2.45·10^6	0.453	0.9937	5.476	4.68	0.9952	4.32·10^4	2.02·10^8	0.9703

Table 4. Comparison of the Adsorption Capacities of MO onto Various Adsorbents

adsorbents	q_m mol·kg^{-1}	references
Mg−Al LDH	0.453	this work
hypercrosslinked polymeric adsorbent	0.217	45
banana peels	0.064	46
orange peels	0.063	46
activated carbon	0.029	47
modified sporopollenin	0.016	48
NH_3^+ MCM-41	1.120	49
polyaniline microspheres	0.472	15

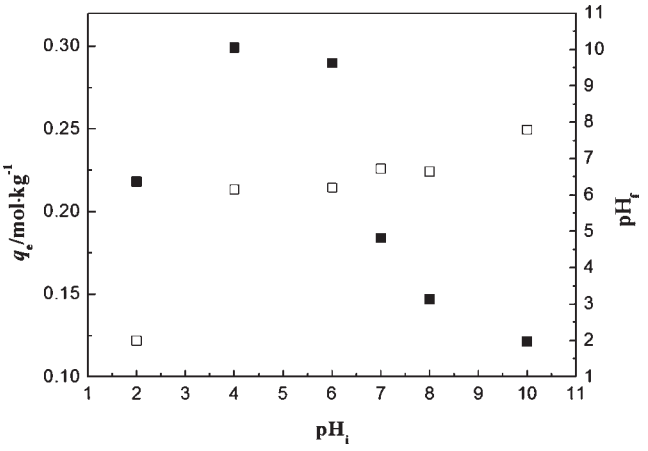

Figure 8. Equilibrium adsorption capacity q_e (square) and pH_f (opened square) versus pH_i for the adsorption of MO onto the Mg−Al LDH. pH_f: final pH values, pH_i: initial pH values.

isotherms (Table 3), suggesting that the Temkin isotherm model does not fit equilibrium data as well as the Langmuir and Freundlich isotherm models.

3.5. Effect of Initial pH. The solution pH is an important parameter controlling the dye adsorption process, since it can affect the surface charge of the adsorbent, the ionization degree of the different pollutants, the dissociation of functional groups on the active sites of the adsorbent, and the structure of the dye molecule. Figure 8 shows the effect of initial pH on the adsorption capacity of MO onto the Mg−Al LDH. The adsorption capacity of MO increased from (0.218 to 0.299) mol·kg^{-1} with increasing pH from (2.0 to 4.0) and decreased slightly in the pH range of (4.0 to 6.0). Afterword, adsorption capacity quickly decreased when the pH was above 6.0. Obviously, MO adsorption closely depends on the solution pH. The point of zero charge (pH_{PZC}) of the Mg−Al LDH is an important

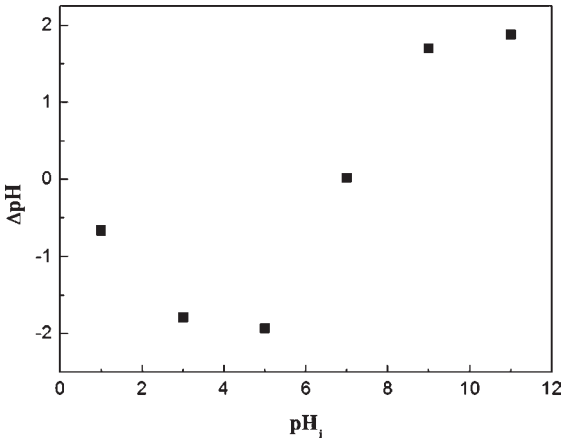

Figure 9. Plot of ΔpH versus pH_i for the determination of point of zero charge of the Mg−Al LDH. ΔpH: the difference between the initial and final pH values, pH_i: initial pH values.

characteristic that determines the pH at which the surface has net electrical neutrality and is therefore assessed by a solid addition method. As shown in Figure 9, the pH_{PZC} of the LDH was estimated to be about 6.98, which is consistent with the reported values (6.8 to 8.9).[55,56] This means that the surface charge of Mg−Al LDH was positive when pH < pH_{PZC} and negative when pH > pH_{PZC}. Therefore, at a solution pH lower than pH_{PZC}, the electrostatic attraction was expected to occur between the positively charged active adsorption sites and anionic dye molecule, accounting for the enhanced adsorption of dye. It should be mentioned that the decrease in adsorption capacity with decreasing pH in the low pH range (pH < 4) may be due to the dissolution of Mg−Al LDH in the low pH solutions, consistent with the reported results in literature. In contrast, the surface of the Mg−Al LDH may acquire negative charges at a solution pH higher than pH_{PZC}. The competitive effects of OH^- ions and the electrostatic repulsion between the anionic dye molecules and the negatively charged active adsorption sites on the Mg−Al LDH would result in a decrease in the adsorption capacity. Figure 8 also shows the relationship between the initial and final pH for MO adsorption, which demonstrates the pH values change during the adsorption process. At low initial pH (pH_i), the final pH values (pH_f) are higher than pH_i values, which is due to the protonation and/or the dissolution of LDH.[57,58] When the pH_i was between 7.0 and 10.0, the pH_f would be in the range of (6.7 to 7.8), indicating a buffering capacity caused by the adsorbent.[59]

4. CONCLUSION

In summary, we have demonstrated the efficient adsorptive removal of MO from aqueous solution with the hydrothermal

synthesized Mg−Al LDH. The effects of initial dye concentration, contact time, and solution on the adsorption capacity of MO onto the Mg−Al LDH were systematically studied. It was found that the adsorption of MO onto the Mg−Al LDH was highly pH-dependent. The adsorption rates of MO onto the Mg−Al LDH were considerably rapid within the first $1.8 \cdot 10^3$ s for all of the initial dye concentrations, and it reached equilibrium around approximately $7.2 \cdot 10^3$ s. The adsorption kinetic studies revealed that the adsorption process followed the pseudosecond-order kinetic model. The equilibrium data were described by various isotherm models such as Langmuir, Freundlich, and Temkin isotherm models among which Langmuir and Freundlich fit the experimental data well. The monolayer adsorption capacity of the Mg−Al LDH toward MO was found to be 0.453 $mol \cdot kg^{-1}$. This study indicated that the LDH could be used as a potential adsorbent for the removal of anionic dye in wastewaters.

AUTHOR INFORMATION

Corresponding Author

*E-mail: ah_aihong@163.com. Tel.: 86-817-2568081.

ACKNOWLEDGMENT

This work was supported by Open Project of Chemical Synthesis and Pollution Control Key Laboratory of Sichuan Province (11CSPC-(1-7)), Program for Scientific and Technological Innovative Team in Sichuan Provincial Universities (2010008), and Program for Scientific Research Innovation Team of China West Normal University.

REFERENCES

(1) Li, S. F. Removal of crystal violet from aqueous solution by sorption into semi-interpenetrated networks hydrogels constituted of poly(acrylic acid-acrylamide-methacrylate) and amylose. *Bioresour. Technol.* **2010**, *101*, 2197–2202.

(2) Bao, N.; Li, Y.; Wei, Z. T.; Yin, G. B.; Niu, J. J. Adsorption of dyes on hierarchical mesoporous TiO_2 fibers and its enhanced photocatalytic properties. *J. Phys. Chem. C* **2011**, *115*, 5708–5719.

(3) Kornaros, M.; Lyberatos, G. Biological treatment of wastewaters from a dye manufacturing company using a trickling filter. *J. Hazard. Mater.* **2006**, *136*, 95–102.

(4) Lee, J. W.; Choi, S. P.; Thiruvenkatachari, R.; Shim, W. G.; Moon, H. Submerged microfiltration membrane coupled with alum coagulation/powder activated carbon adsorption for complete decolorization of reaction dye. *Water Res.* **2006**, *40*, 435–444.

(5) Selcuk, H. Decolorization, detoxification of textile wastewater by ozonation and coagulation processes. *Dyes Pigm.* **2005**, *64*, 217–222.

(6) Dutta, K.; Mukhopadhyaya, S.; Bhattacharjee, S.; Chaudhuri, B. Chemical oxidation of methylene blue using a Fenton-like reaction. *J. Hazard. Mater.* **2001**, *84*, 57–71.

(7) Buonomenna, M. G.; Gordano, A.; Golemme, G.; Drioli, E. Preparation, characterization and use of PEEKWC nanofiltration membranes for removal of Azur B dye from aqueous media. *React. Funct. Polym.* **2009**, *69*, 259–263.

(8) Liu, C. H.; Wu, J. S.; Chiu, H. C.; Suen, S. Y.; Chu, K. H. Removal of anionic reactive dyes from water using anion exchange membranes as adsorbers. *Water Res.* **2007**, *41*, 1491–1500.

(9) Muruganandham, M.; Swaminathan, M. TiO_2-UV photocatalytic oxidation of reactive yellow 14: effect of operational parameters. *J. Hazard. Mater.* **2006**, *135*, 78–86.

(10) Arami, M.; Yousefi-Limaee, N.; Mahmoodi, N. M.; Salman-Tabrizi, N. Equilibrium and kinetics studies for the adsorption of direct and acid dyes from aqueous solution by soy meal hull. *J. Hazard. Mater.* **2006**, *B135*, 171–179.

(11) Pendleton, P.; Wu, S. H. Kinetics of dodecanoic acid adsorption from caustic solution by activated carbon. *J. Colloid Interface Sci.* **2003**, *226*, 245–250.

(12) Faki, A.; Turan, M.; Ozdemir, O.; Turan, A. Z. Analysis of fixed-bed column adsorption of Reactive Yellow 176 onto surfactant-modified zeolite. *Ind. Eng. Chem. Res.* **2008**, *47*, 6999–7004.

(13) Pengthamkeerati, P.; Satapanajaru, T.; Singchan, O. Sorption of reactive dye from aqueous solution on biomass fly ash. *J. Hazard. Mater.* **2008**, *153*, 1149–1156.

(14) Ai, L. H.; Zhou, Y.; Jiang, J. Removal of methylene blue from aqueous solution by montmorillonite/$CoFe_2O_4$ composite with magnetic separation performance. *Desalination* **2011**, *266*, 72–77.

(15) Ai, L. H.; Jiang, J.; Zhang, R. Uniform polyaniline microspheres: A novel adsorbent for dye removal from aqueous solution. *Synth. Met.* **2010**, *160*, 762–767.

(16) Pavan, F. A.; Mazzocato, A. C.; Gushikem, Y. Removal of methylene blue dye from aqueous solutions by adsorption using yellow passion fruit peel as adsorbent. *Bioresour. Technol.* **2008**, *99*, 3162–3165.

(17) Xiang, X.; Hima, H. I.; Wang, H.; Li, F. Facile synthesis and catalytic properties of nickel-based mixed-metal oxides with mesopore networks from a novel hybrid composite precursor. *Chem. Mater.* **2008**, *20*, 1173–1182.

(18) Gu, Z.; Thomas, A. C.; Xu, Z. P.; Campbell, J. H.; Lu, G. Q. In vitro sustained release of LMWH from MgAl-layered double hydroxide nanohybrids. *Chem. Mater.* **2008**, *20*, 3715–3722.

(19) Williams, G. R.; O'Hare, D. Towards understanding, control and application of layered double hydroxide chemistry. *J. Mater. Chem.* **2006**, *16*, 3065–3074.

(20) Oh, J.-M.; Biswick, T. T.; Choy, J.-H. Layered nanomaterials for green materials. *J. Mater. Chem.* **2009**, *19*, 2553–2563.

(21) Cavani, F.; Trifiro, F.; Vaccari, A. Hydrotalcite-type anionic clays: Preparation, properties and applications. *Catal. Today* **1991**, *11*, 173–301.

(22) Duan, X.; Evans, D. G. *Layered Double Hydroxide*; Springer: Berlin, 2006; Vol. 119.

(23) Gao, Z. Y.; Du, B.; Zhang, G. Y.; Gao, Y.; Li, Z. J.; Zhang, H.; Duan, X. Adsorption of pentachlorophenol from aqueous solution on dodecylbenzenesulfonate modified nickel-titanium layered double hydroxide nanocomposites. *Ind. Eng. Chem. Res.* **2011**, *50*, 5334–5345.

(24) El Gaini, L.; Lakraimi, M.; Sebbar, E.; Meghea, A.; Bakasse, M. Removal of indigo carmine dye from water to Mg-Al-CO_3 calcined layered double hydroxides. *J. Hazard. Mater.* **2009**, *161*, 627–632.

(25) Chen, S. L.; Xu, Z. P.; Zhang, Q.; Max Lu, G. Q.; Hao, Z. P.; Liu, S. M. Studies on adsorption of phenol and 4-nitrophenol on MgAl-mixed oxide derived from MgAl-layered double hydroxide. *Sep. Purif. Technol.* **2009**, *67*, 194–200.

(26) Li, Y. J.; Gao, B. Y.; Wu, T.; Sun, D. J.; Li, X.; Wang, B.; Lu, F. J. Hexavalent chromium removal from aqueous solution by adsorption on aluminum magnesium mixed hydroxide. *Water Res.* **2009**, *43*, 3067–3075.

(27) Xing, K.; Wang, H. Z.; Guo, L. G.; Song, W. D.; Zhao, Z. P. Adsorption of tripolyphosphate from aqueous solution by Mg-Al-CO_3-layered double hydroxides. *Colloids Surf., A* **2008**, *328*, 15–20.

(28) Sun, G. B.; Sun, L. N.; Wen, H.; Jia, Z. Q.; Huang, K. L.; Hu, C. W. From layered double hydroxide to spinel nanostructures: Facile synthesis and characterization of nanoplatelets and nanorods. *J. Phys. Chem. B* **2006**, *110*, 13375–13380.

(29) Ai, L. H.; Huang, H. Y.; Chen, Z. L.; Wei, X.; Jiang, J. Activated carbon/$CoFe_2O_4$ composites: Facile synthesis, magnetic performance and their potential application for the removal of malachite green from water. *Chem. Eng. J.* **2010**, *156*, 243–249.

(30) Ai, L. H.; Jiang, J. Fast removal of organic dyes from aqueous solutions by AC/ferrospinel composite. *Desalination* **2010**, *262*, 134–140.

(31) Ghaedi, M.; Hassanzadeh, A.; Kokhdan, S. N. Multiwalled carbon nanotubes as adsorbents for the kinetic and equilibrium study of the removal of Alizarin Red S and Morin. *J. Chem. Eng. Data* **2011**.

(32) Lagergren, S. About the theory of so-called adsorption of soluble substances. *K. Sven. Vetenskapsakad. Handl.* **1898**, *24*, 1–39.
(33) Ho, Y. S.; McKay, G. Sorption of dye from aqueous solution by peat. *Chem. Eng. J.* **1998**, *70*, 115–124.
(34) Benselka-Hadj Abdelkader, N.; Bentouami, A.; Derriche, Z.; Bettahar, N.; de Ménorval, L.-C. Synthesis and characterization of Mg-Fe layer double hydroxides and its application on adsorption of Orange G from aqueous solution. *Chem. Eng. J.* **2011**, *169*, 231–238.
(35) Chen, H.; Dai, G. L.; Zhao, J.; Zhong, A. G.; Wu, J. Y.; Yan, H. Removal of copper(II) ions by a biosorbent-*Cinnamomum camphora* leaves powder. *J. Hazard. Mater.* **2010**, *177*, 228–236.
(36) Cheung, C. W.; Porter, J. F.; McKay, G. Sorption kinetic analysis for the removal of cadmium ions from effluents using bone char. *Water Res.* **2001**, *35*, 605–612.
(37) Weber, W. J., Jr.; Morris, J. C. Kinetics of adsorption on carbon from solution. *J. Sanit. Eng. Div. Am. Soc., Civ. Eng.* **1963**, *89*, 31–60.
(38) Arami, M.; Yousefi Limaee, N.; Mahmoodi, N. M. Evaluation of the adsorption kinetics and equilibrium for the potential removal of acid dyes using a biosorbent. *Chem. Eng. J.* **2008**, *139*, 2–10.
(39) Ugurlu, M. Adsorption of a textile dye onto activated sepiolite. *Microporous Mesoporous Mater.* **2009**, *119*, 276–283.
(40) Boyd, G. E.; Adamson, A. W.; Meyers, L. S. The exchange adsorption of ions from aqueous solutions by organic zeolites: II kinetics. *J. Am. Chem. Soc.* **1947**, *69*, 2836–2848.
(41) Giles, C. H.; MacEwan, T. H.; Nakhwa, S. M.; Smith, D. Studies on adsorption. XI. A system of classification of solution adsorption isotherms and its use in diagnosis of adsorption mechanisms and in measurement of specific surface areas of solids. *J. Chem. Soc. London* **1960**, *56*, 1973–2993.
(42) Langmuir, I. The constitution and fundamental properties of solids and liquids. *J. Am. Chem. Soc.* **1916**, *38*, 2221–2295.
(43) Freundlich, H. M. F. Over the adsorption in solution. *Z. Phys. Chem.* **1906**, *57*, 385–471.
(44) Temkin, M. J.; Pyzhev, V. Kinetics of ammonia synthesis on promoted iron catalysts. *A. Physiochim. URSS* **1940**, *12*, 217–222.
(45) Huang, J.-H.; Huang, K.-L.; Liu, S.-Q.; Wang, A.-T.; Yan, C. Adsorption of Rhodamine B and methyl orange on a hypercrosslinked polymeric adsorbent in aqueous solution. *Colloids Surf., A* **2008**, *330*, 55–61.
(46) Singh, K. P.; Mohan, D.; Sinha, S.; Tondon, G. S.; Gosh, D. Color removal from wastewater using low-cost activated carbon derived from agricultural waste material. *Ind. Eng. Chem. Res.* **2003**, *42*, 1965–1976.
(47) Annadurai, G.; Juang, R.; Lee, D. Use of cellulose-based wastes for adsorption of dyes from aqueous solutions. *J. Hazard. Mater.* **2002**, *B92*, 263–274.
(48) Ayar, A.; Gezici, O.; Kucukosmanoglu, M. Adsorptive removal of methylene blue and methyl orange from aqueous media by carboxylated diaminoethane sporopollenin: on the usability of an aminocarboxilic acid functionality bearing solidstationary phase in column techniques. *J. Hazard. Mater.* **2007**, *146*, 186–193.
(49) Qin, Q.; Ma, J.; Liu, K. Adsorption of anionic dyes on ammonium-functionalized MCM-41. *J. Hazard. Mater.* **2009**, *162*, 133–139.
(50) Weber, T. W.; Chakravorti, R. K. Pore and solid diffusion models for fixed-bed adsorbers. *AIChE J.* **1974**, *20*, 228–238.
(51) McKay, G. Adsorption of dyestuffs from aqueous solution with activated carbon. I. Equilibrium and batch contact time studies. *J. Chem. Technol. Biotechnol.* **1982**, *32*, 759–772.
(52) Xiong, L.; Yang, Y.; Mai, J.; Sun, W.; Zhang, C.; Wei, D.; Chen, Q.; Ni, J. Adsorption behavior of methylene blue onto titanate nanotubes. *Chem. Eng. J.* **2010**, *156*, 313–320.
(53) Duran, C.; Ozdes, D.; Gundogdu, A.; Senturk, H. B. Kinetics and isotherm analysis of basic dyes adsorption onto almond shell (*Prunus dulcis*) as a low cost adsorbent. *J. Chem. Eng. Data* **2011**, *56*, 2136–2147.
(54) Chen, S. H.; Yue, Q. Y.; Gao, B. Y.; Li, Q.; Xu, X. Removal of Cr(VI) from aqueous solution using modified corn stalks: Characteristic, equilibrium, kinetic and thermodynamic study. *Chem. Eng. J.* **2011**, *168*, 909–917.
(55) Yang, L.; Shahrivari, Z.; Liu, P. K. T.; Sahimi, M.; Tsotsis, T. T. Removal of trace levels of arsenic and selenium from aqueous solutions by calcined and uncalcined layered double hydroxides (LDH). *Ind. Eng. Chem. Res.* **2005**, *44*, 6804–6815.
(56) Das, D. P.; Das, J.; Parida, K. Physicochemical characterization and adsorption behavior of calcined Zn/Al hydrotalcite-like compounds (HTLs) towards removal of fluoride from aqueous solution. *J. Colloid Interface Sci.* **2003**, *261*, 213–220.
(57) Sathishkumar, M.; Binupriya, A. R.; Kavitha, D.; Selvakumar, R.; Jayabalan, R.; Choi, J. G.; Yun, S. E. Adsorption potential of maize cob carbon for 2,4-dichlorophenol removal from aqueous solutions: Equilibrium, kinetics and thermodynamics modeling. *Chem. Eng. J.* **2009**, *147*, 265–271.
(58) Mane, V. S.; Babu, P. V. V. Studies on the adsorption of brilliant green dye from aqueous solution onto low-cost NaOH treated saw dust. *Desalination* **2011**, No. 273, 321–329.
(59) Lim, S. F.; Zheng, Y. M.; Zou, S. W. Characterization of copper adsorption onto an alginate encapsulated magnetic sorbent by a combined FT-IR, XPS, and mathematical modeling Study. *Environ. Sci. Technol.* **2008**, *42*, 2551–2556.